Six-Coordinate Ln(III) Complexes with Various Coordination Geometries Showing Distinct Magnetic Properties

Table S1. Selected bond distances [Å] and angles [°] for complexes **1Dy**, **1Er**, and **2Dy**.

1Dy		**1Er**		**2Dy**	
Dy1-O1	2.167(3)	Er1-O1	2.146(5)	Dy1-O1	2.208(3)
Dy1-O2	2.154(2)	Er1-O2	2.128(4)	Dy1-O2	2.182(3)
Dy1-O3	2.144(3)	Er1-O3	2.123(5)	Dy1-O3	2.275(3)
Dy1-N1	2.606(3)	Er1-N1	2.567(5)	Dy1-O4	2.170(3)
Dy1-N2	2.481(3)	Er1-N2	2.462(6)	Dy1-N3	2.515(4)
Dy1-N3	2.446(3)	Er1-N3	2.411(4)	Dy1-N4	2.662(4)
O1-Dy1-N1	71.48(10)	O1-Er1-N1	71.97(18)	O1-Dy1-O2	89.08(12)
O2-Dy1-N2	74.90(9)	O2-Er1-N2	76.17(18)	O3-Dy1-O4	155.23(12)
O3-Dy1-N3	74.43(9)	O3-Er1-N3	75.46(17)	N3-Dy1-N4	68.88(12)
O1-Dy1-O2	142.05(11)	O1-Er1-O2	140.6(2)	O1-Dy1-O3	96.78(11)
O2-Dy1-O3	132.32(10)	O2-Er1-O3	132.89(19)	O2-Dy1-N3	166.62(12)
O1-Dy1-O3	84.63(11)	O1-Er1-O3	84.9(2)	O1-Dy1-N4	171.36(13)
Dy···Dy	10.8822(15)	Er···Er	10.9407(12)	Dy···Dy	10.3614(9)

Table S2. Lanthanide geometry analysis by SHAPE software for **1Dy**, **1Er**, and **2Dy**.

Geometry	Hexagon (D_{6h})	Pentagonal pyramid (C_{5v})	Octahedron (O_h)	Trigonal prism (D_{3h})
1Dy	27.53	11.96	18.20	**2.36**
1Er	27.97	12.40	17.59	**2.06**
2Dy	27.79	24.33	**1.70**	13.33

Table S3. Best-fit parameters for the Arrhenius plots of **1Dy** and **1Er**.

Compound	U_{eff} / K	τ_0 / s	τ_{QTM} / ms	AH^2	C ($s^{-1}K^{-n}$)	n
1Dy	31.40	3.56×10^{-4}	0.303	–	1.375	2.997
1Er (400 Oe)	23.96	5.46×10^{-8}	0.414	–	0.0059	10.68

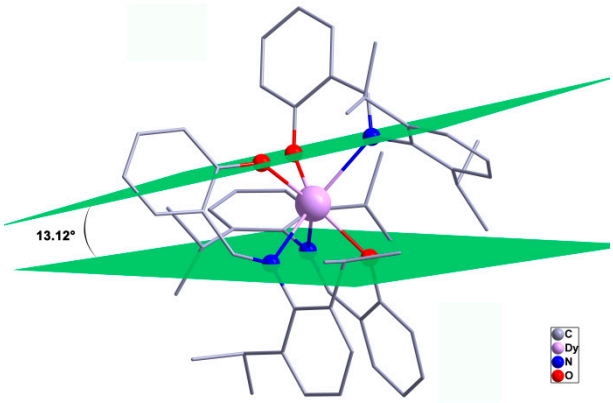

Figure S1. X-ray structures of complex **1Dy**. The green planes represent the coordination planes with labeled dihedral angle (θ). Hydrogen atoms have been omitted for clarity.

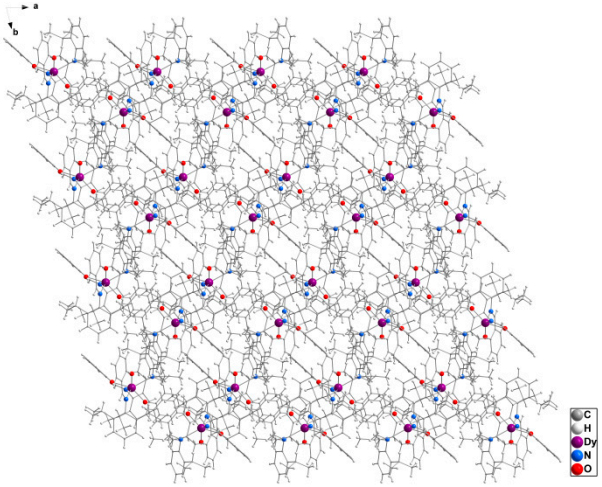

Figure S2. Packing diagram of **1Dy** viewed along the *c*-axis.

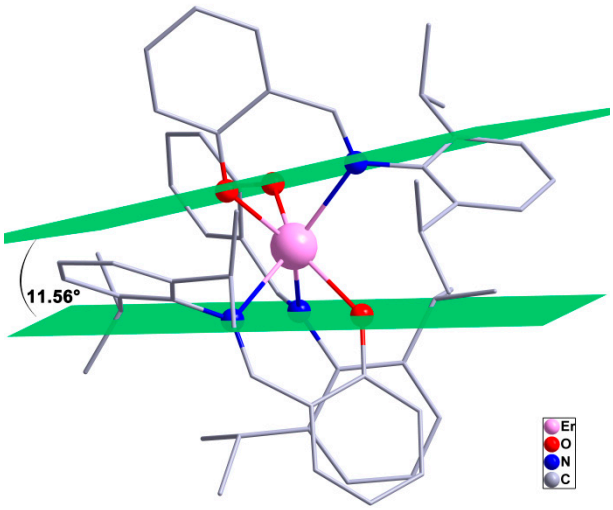

Figure S3. X-ray structures of complexes **1Er**. The green planes represent the coordination planes with labeled dihedral angle (θ). Hydrogen atoms have been omitted for clarity.

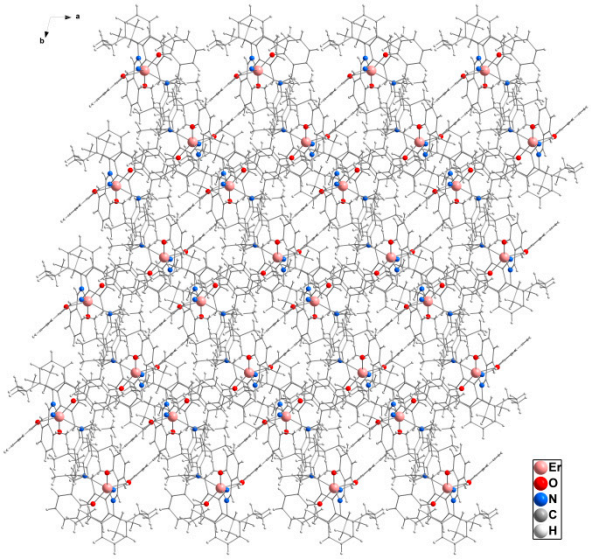

Figure S4. Packing diagram of **1Er** viewed along the *c*-axis.

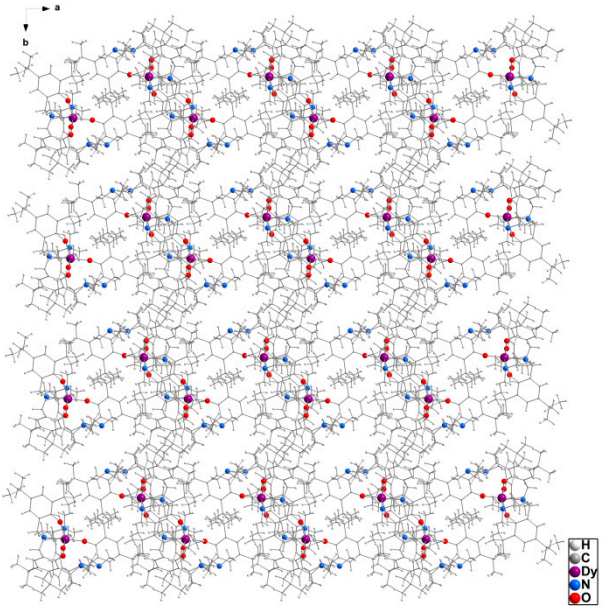

Figure S5. Packing diagram of **2Dy** viewed along the *c*-axis.

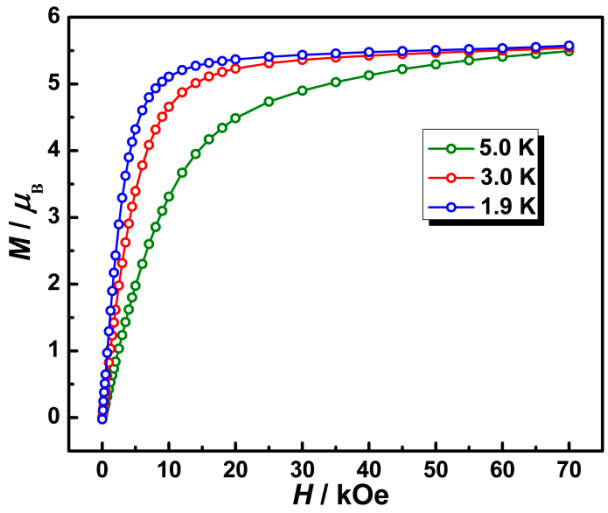

Figure S6. Molar magnetization (*M*) versus field (*H*) for complex **1Dy** at 1.9, 3.0, and 5.0 K.

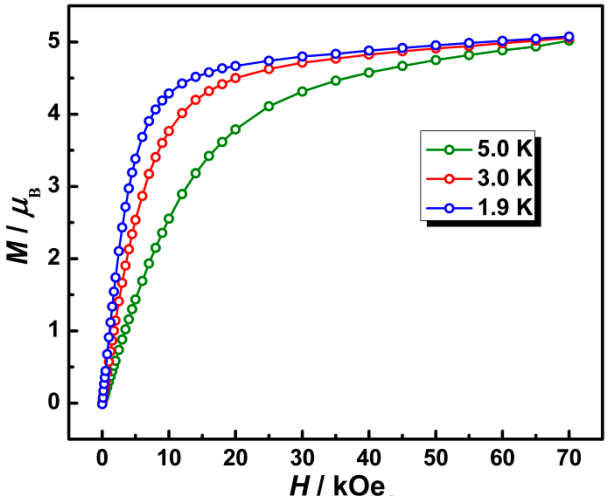

Figure S7. Molar magnetization (*M*) versus field (*H*) for complex **1Er** at 1.9, 3.0, and 5.0 K.

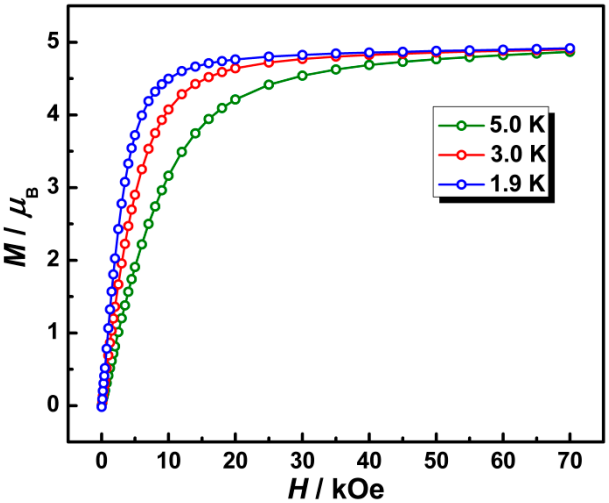

Figure S8. Molar magnetization (*M*) versus field (*H*) for complex **2Dy** at 1.9, 3.0, and 5.0 K.

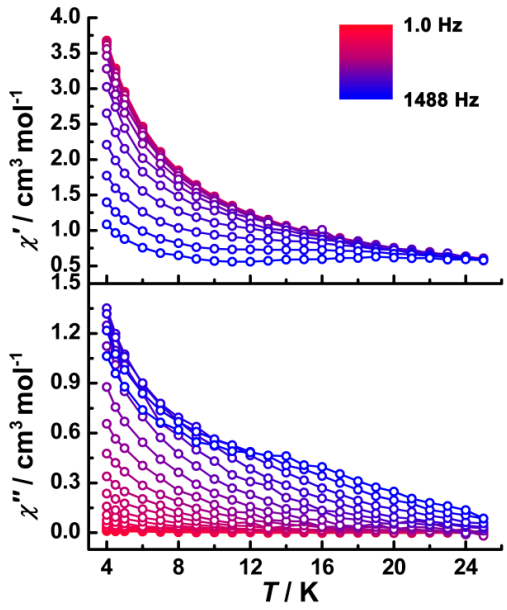

Figure S9. Temperature-dependent in-phase (χ') and-out-of phase (χ'') ac susceptibilities for complex **1Dy** at indicated frequencies under zero dc field.

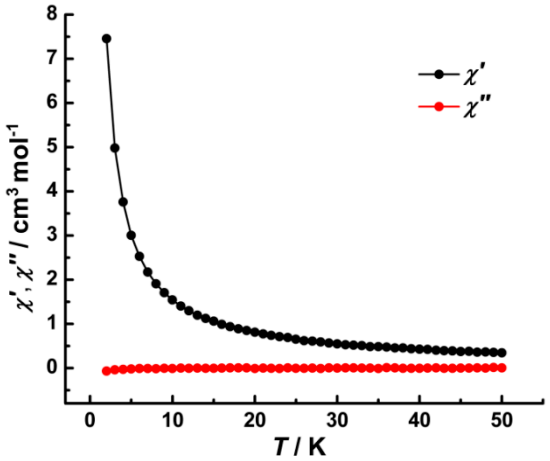

Figure S10. Temperature-dependent in-phase (χ') and out-of-phase (χ'') ac susceptibilities for complex **1Er** under zero dc field.

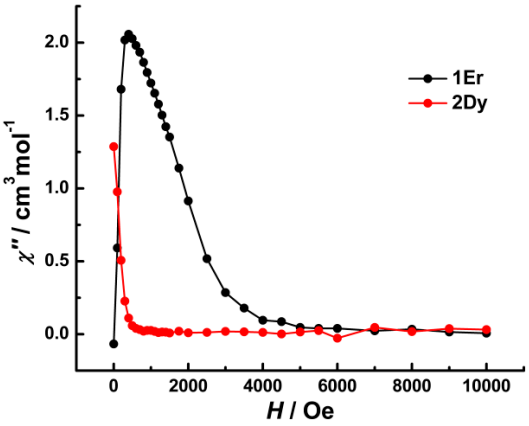

Figure S11. The field dependence of the out-of-phase signals of **1Er** and **2Dy** on applied dc field strength at 1.9 K and 997 Hz.

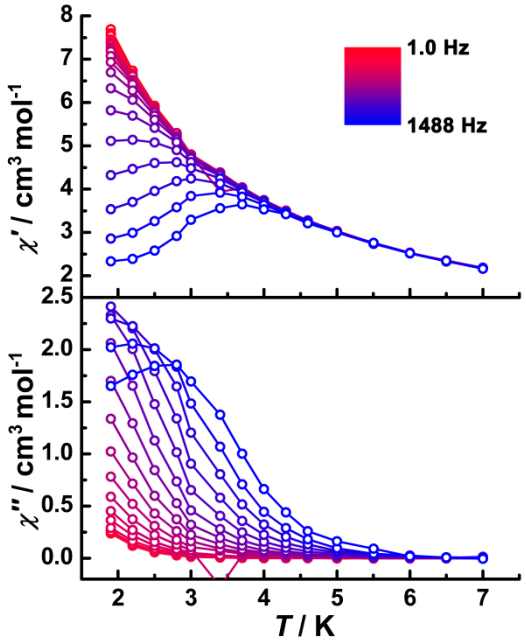

Figure S12. Temperature-dependent in-phase (χ') and out-of-phase (χ'') ac susceptibilities for complex **1Er** under 400 Oe dc field.

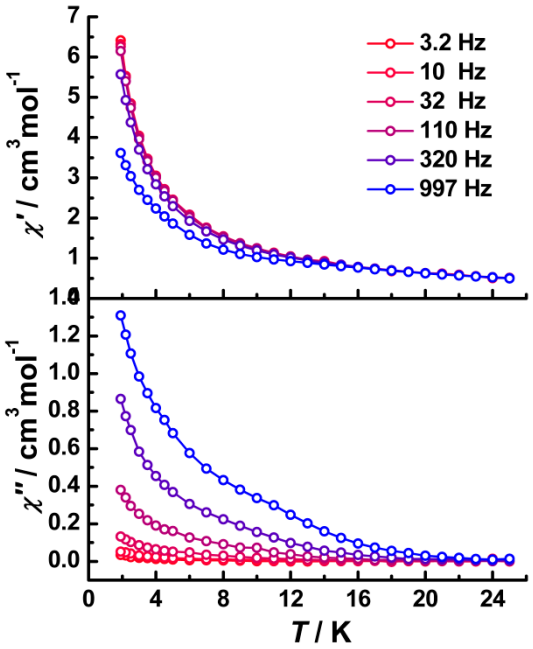

Figure S13. Temperature-dependent in-phase (χ') and out-of-phase (χ'') ac susceptibilities for complex **2Dy** under zero dc field.